PROCEEDINGS, 50th Workshop on Geothermal Reservoir Engineering
Stanford University, Stanford, California, February 10-12, 2025
SGP-TR-229

Pore-Scale and Site-Scale Modeling of Granular Particle-based Lost Circulation Management for Geothermal Drilling

Pramod Bhuvankar[1], Matthew T Reagan[1], Seiji Nakagawa[1], and Patrick Dobson[1]

[1]Lawrence Berkeley National Laboratory, Berkeley, CA 94720

<pbhuvankar@lbl.gov>

Keywords: Lost Circulation Management; Drilling Technology; Granular Particles; LCM; CFD; Immersed Boundary Method; TOUGH+

ABSTRACT

Circulation Losses are common in geothermal drilling when a high permeability zone or natural fractures are encountered. The deployment of Lost Circulation Materials (LCM) is a commonly used method to plug fractures and reduce the loss of circulation fluids. In the current work we simulate LCM-based management of circulation loss, at the pore and reservoir scales. For the pore-scale study we use a 2D, Immersed Boundary Method-based CFD technique to simulate the entry-plugging behavior of round LCM particles at the entry of a single fracture. Our simulations with LCM particle sizes 0.18 mm, 0.22 mm, and 0.33 mm, and a fracture aperture of 0.75 mm show that coarser particles form unstable bridges at the fracture entry point. The LCM particle flow is driven by a pressure differential ΔP imposed across the fracture entry. For ΔP values up to 22 MPa, two distinct phases, namely, the bridging and free flowing phases are observed at the fracture entry point. The 0.33 mm size results in the best performance with an effective fracture permeability of 8×10^{-14} m^2. Our site-scale simulations of LCM deployment using TOUGH+ show that with the selection of suitable LCM size, significant and quick reduction in circulation losses can be achieved.

1. INTRODUCTION

Circulation Loss (CL) into high-permeability zones during drilling is a challenge in enhanced geothermal systems. The Non-Productive Time resulting from the loss of circulation fluids into natural or induced fractures during drilling can significantly add to the cost (Feng et al., 2017a). CL is known to cost up to 10% of the total project cost in geothermal projects in the US (Sun *et al.,* 2021). If left unmitigated, in extreme cases, CL can lead to severe problems such as blowouts and abandonment of the project (Sun *et al.,* 2021). Therefore, Lost Circulation Management has been a topic of ongoing research in the field of drilling technologies. A comprehensive review of the existing technologies for the management of circulation loss can be found in Sun *et al.* (2021). These technologies include the deployment of particulate Lost Circulation Materials (LCM) (Kibikas *et al.*, 2024), shear-sensitive fluids (Nazemi *et al.,* 2024), and more advanced technologies like shape memory polyurethane (Lashkari *et al.*, 2023). Additionally, several smart materials and gels have been proposed as effective agents for managing CL (Sun *et al.*, 2021). The objective of these technologies is to plug fractures and high permeability zones that cause CL during drilling.

The most common of the mentioned technologies is the deployment of bridging-plugging particulate LCM. These are fibrous, granular, or flaky materials like cotton-seed hull, mica, and resin flakes, that are readily available (Kibikas *et al.*, 2024). In practice, the particle size distribution of these LCMs is related to the mean fracture aperture by correlations such as Abram's one-third rule (Abrams *et al.* 1977), Alsaba method (Alsaba *et al.*, 2017), and Vicker's rule (Vicker *et al.*, 2006). Researchers have used lab-scale experimental methods and modeling techniques to study the efficacy of various types of granular LCM. Kang *et al.* (2023) showed through lab experiments that when used in combination with one another, fibrous and granular LCM exhibit high efficiency in plugging millimeter-scale fractures. They also establish the role of elastic properties and deformation of LCM particles in governing the stability of the plugged zones within the fracture. Wang et al.'s (Wang) experiments show two mechanisms of permeability reduction exhibited by LCM, namely, throat and mouth sealing. Figures 1 (a) and (b) illustrate these mechanisms, respectively. Both-throat plugging (Razavi et al., 2016) and mouth sealing (Loeppke 1990, Kibikas et al., 2024) were observed by various research groups. Jeenakorn *et al.* (2017), observed mouth sealing behavior in the case of coarse LCM particles. Due to uncertainties associated with the fracture aperture distribution in practice, both mechanisms need to be studied.

The impacts of parameters like particle shape, fracture roughness, material and thermal properties of the LCM, on circulation loss is an ongoing topic of research in drilling technologies. Lee and Dahi Taleghani conducted CFD-DEM simulations (Lee *et al.*, 2020, 2021, 2022) to study the effect of friction and thermal degradation on LCM performance. Their CFD technique has been used to study the impact of particle size, and fibrous nature on circulation loss in fractures (Lin *et al.*, 2022, 2024). While much attention has been paid in literature to the throat plugging phenomenon, more investigations are required on the mouth sealing behavior of coarser LCM. In the current work we use 2D Immersed Boundary technique (Bhuvankar *et al.*, 2022, 2023) in conjunction with CFD to understand the flow behavior of uniform-sized granular LCM particles near the entry of a single fracture. We simulate particulate flows with three particle sizes and a 0.75 mm fracture aperture with a focus on the mouth-sealing characteristics.

We also conduct reservoir scale simulations of LCM flow using LBNL's simulator TOUGH+ (Moridis *et al*., 2014). We create a reservoir-scale model of fluid flow out of an uncased wellbore into a fractured fluid-entry zone. While flow of drilling muds within porous and/or fractured formations have been modeled using various reservoir simulators (Feng *et al*., 2007a;b), this capability has not been implemented

in the TOUGH family of codes, developed at the Lawrence Berkeley National Laboratory (LBNL) within the original focus on geothermal reservoir engineering. We implement density and viscosity functions for muds in the TOUGH+RealGasBrine code framework and include permeability reduction functions to represent the effect of LCMs. Fluid flow changes due to the presence of the LCMs (represented by the permeability reductions) are estimated, and the pressure response of the wellbore and the volume of lost fluid are simulated and assessed.

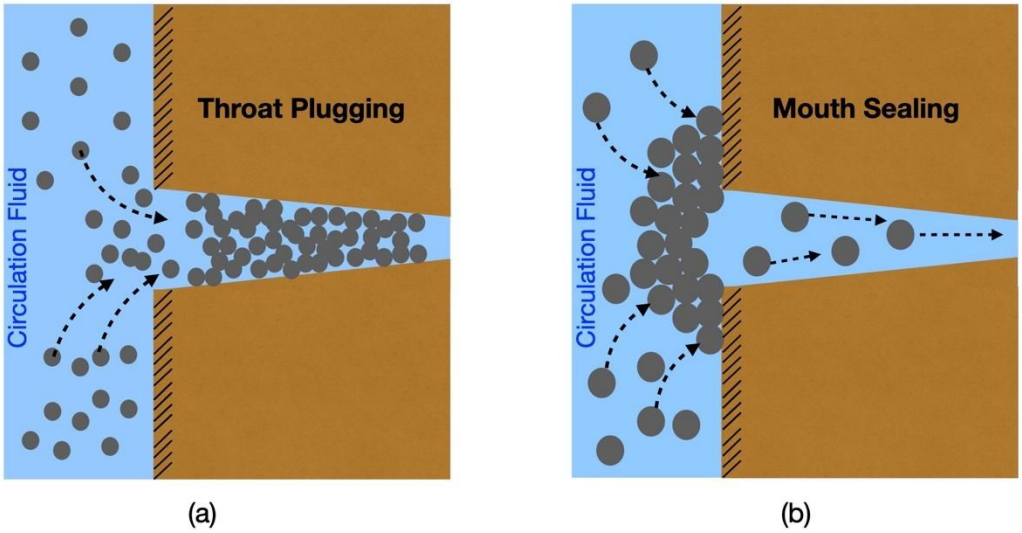

Figure 1: (a) Throat plugging behavior by granular LCM particles. (b) Mouth sealing behavior by coarser LCM particles.

2. PORE-SCALE MODELING

In the current work, we assume the pore-scale particulate flow to be incompressible and isothermal. Fluid properties such as density and viscosity are assumed to be constant near the fracture opening. The LCM particles are assumed to have uniform size and a round shape. We assume particle-particle and particle-rock collisions to be inelastic in nature.

2.1 Governing Equations and Problem Setup

The mass and momentum transport are described by the following equations

$$\nabla . u = 0 \tag{1}$$

$$\rho\left(\partial_t u + \nabla . (uu)\right) = -\nabla p + \nabla . \{\mu(\nabla u + (\nabla u)^T)\} + \rho g + \rho F \tag{2}$$

In the above equations, $\boldsymbol{u}$, ρ, and μ are the Eulerian velocity field, density, and dynamic viscosity of the fluid, respectively. $\boldsymbol{F}$ is the immersed boundary force that is used to enforce solid body behavior in the parts of the computational domain occupied by LCM particles and the rock zone. Figure 2 shows the solid and fluid zones in the computational domain.

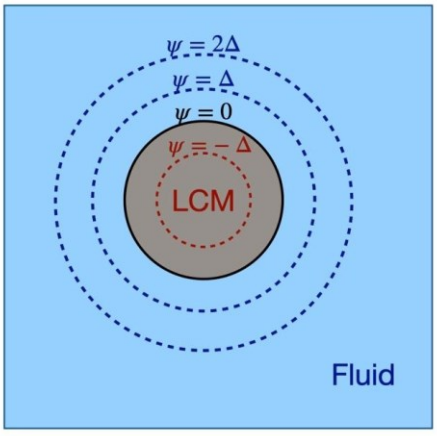

Figure 2: Schematic of the LCM and fluid parts of the computational domain defined by distance function.

To distinguish between said zones we use the distance function ψ. ψ is the shortest signed distance of a point from a solid-fluid interface. In the above equations, $\boldsymbol{u}$, ρ, and μ are the Eulerian velocity field, density, and dynamic viscosity of the fluid, respectively. $\boldsymbol{F}$ is the immersed boundary force that is used to enforce solid body behavior in the parts of the computational domain occupied by LCM particles and the rock zone. Figure 2(a) shows the solid and fluid zones in the computational domain. To distinguish between said zones we use the distance function ψ. ψ is the shortest signed distance of a point from a solid-fluid interface. The zero-level set of the distance function is used to represent the solid-fluid interface. We define a color function $c(x)$ as:

$$c(x) = 0.5\left[1 + tanh\left(\frac{2\psi(x)}{\Delta}\right)\right], \tag{3}$$

wherein, Δ is the grid spacing. $c(x)$ is -1 and +1 in the solid and fluid zones, respectively. Both zones are separated by a diffuse interface that is 4Δ thick. The immersed boundary force $F(x)$ in Equation 2, is computed using $c(x)$ by a method described in Bhuvankar *et al.* (2022). The velocity field inside the solid zone is described by rigid-body motion as

$$u(x) = u_i + \omega_i \times (x - x_i) \tag{4}$$

wherein, u_i, ω_i, and x_i are the linear, angular velocities, and center of mass location of the LCM particle *i,* respectively. For a continuous force field $\boldsymbol{F}(\boldsymbol{x})$ we can show that the trajectory and rotation of an LCM particle are given as

$$\frac{du_i}{dt} = g - \frac{1}{(\rho_i - \rho)v_i}\int \quad \rho F dv + \frac{F_{ext}}{m_i} \tag{5}$$

$$I_i \frac{d\omega_i}{dt} = -\frac{\rho_i}{(\rho_i - \rho)}\int \quad \rho(r \times F)dv + \tau_{ext} \tag{6}$$

In Equations 5 and 6, I_i, ω_i, ρ_i, v_i, m_i, F_{ext}, τ_{ext} are the particle moment of inertia, angular velocity, density, volume, mass, sum total of external forces, and torques, respectively. The external forces and torques include those quantities arising from particle-particle and particle-rock contact and collisions. We model contact forces between any two interacting objects using the Hertz-Mindlin model (Nosewicz *et al.,* 2017). Frictional forces are implemented into our particulate flow model using the technique described in Andrade *et al.* (2012). We assume that the coefficients of static and dynamic friction are equal.

Figure 3 shows the problem setup for our pore-scale simulations. LCM particles are made to flow through a single fracture of aperture 0.75 mm. The flow is driven by a pressure difference ΔP imposed between the over-pressured boundaries and the outflow boundary, as depicted in Figure 3. There is an LCM zone, of area 1.56 mm^2 near the fracture entry, wherein all LCM particles are initialized. Particles that leave the computational domain through the outflow boundary are made to re-enter into this zone to maintain a constant particle density. Each rock zone has dimensions 0.75 mm x 0.75 mm and is assumed to be impermeable compared to the fracture. We average the flow velocity over the outflow boundary to compute the instantaneous outflow velocity, which is in turn integrated with time to compute cumulate leakage through the fracture. The time averaged fluid velocity $\langle U \rangle$ at the outlet is used to compute effective entry permeability *k*. We simulate LCM flow with three particle diameters, namely, 0.18 mm, 0.22 mm, and 0.33 mm.

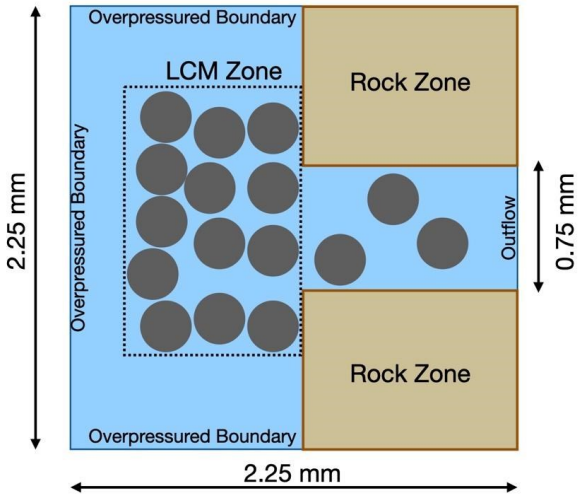

Figure 3: Problem setup, showing the LCM zone, single fracture entry, and pressure boundaries.

ΔP values between 0.05 MPa and 22 MPa are simulated across the three mentioned particle diameters. The densities of the fluid and LCM solid material are taken to be 1000 kg/m3 and 1200 kg/m3, respectively. The fluid viscosity is assumed to be 8.9E-4 Pa-s. The Youngs

modulus and Pascal ratio of the LCM are assumed to be 183 GPa and 0.33, respectively. The coefficients of static and dynamic friction are assumed to be 0.75. A constant LCM particle volume fraction of 0.75 is used throughout this study.

2.2 Pore-Scale Results and Discussion

In all our simulations we observe unstable bridging to be the main mechanism of fracture plugging. Figure 4(a) shows cumulative leakage for the simulation with particle size 0.22 mm with a 2 MPa pressure differential. We observe the cumulative leakage to evolve in step-wise increments. The inner plot in Figure 4(a) shows one bridge formation followed by the subsequent bridge breakage event marked by points A and B. The bridge exhibits sliding motion in between stages A and B. After the breakage of the bridge the fluid accelerates into the fracture causing a steeper increment in cumulative leakage.

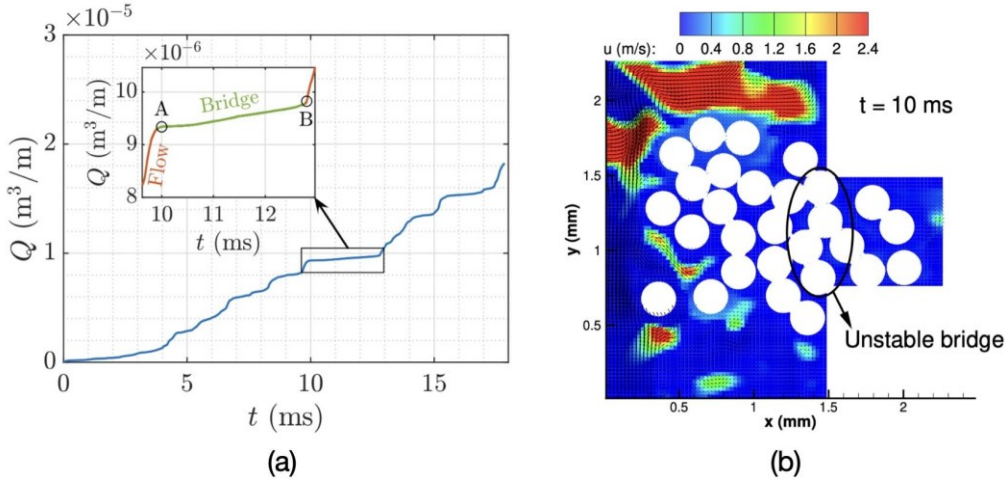

Figure 4: (a) Cumulative fluid leakage as a function of time for the 0.22 mm case with a 2 MPa differential, showing step-wise increments. (b) Velocity contour around the fracture during bridge formation for the 0.22 mm case.

Figure 4(b) shows the *x*-velocity distribution in and around the fracture at stage A of the model. Note the higher velocity magnitude near the top of the computational domain at this stage as the fluid is directed upwards due to the bridge plugging the fracture entry. Figure 5(a) shows the fluid leakage for the three simulated sizes for a pressure difference of 1.6 MPa.

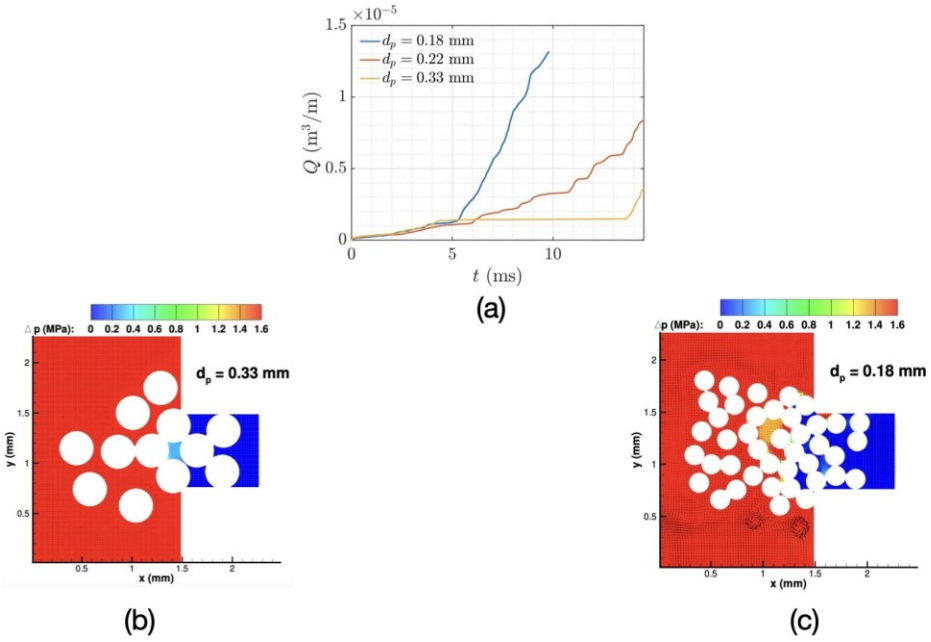

Figure 5: (a) Cumulative fluid leakage plot for 0.18 mm, 0.22 mm, and 0.33 mm cases with a 1.6 MPa differential. Pressure contours during mouth plugging for cases with size (b)0.33 mm and (c) 0.18 mm.

We note that the coarsest particle size, 0.33 mm, shows the best plugging efficiency, and the finest size, 0.18 mm, has the highest leakage. We also note that the bridging phase is most prolonged for the coarsest case of 0.33 mm, followed by the other cases. Bridging is found

in the cases of 0.22 mm and 0.18 mm, but they are more transient compared to the 0.33 mm case. Figures 5(b) and (c) show a sharp differential in the pressure distribution across the bridging structures for 0.33 mm and 0.18 mm. The sharp pressure differential indicates plugging of the fracture entry by mouth plugging. During this mouth plugging stage, the bridging structure is held by the inter-particle static friction forces and the particle-rock static friction forces. When the frictional force between any two particles or a particle and the rock exceeds the static friction limit, this will cause slippage leading to the dislodging of the bridging struction.

Figures 6 (a), (b), and (c) show all the data points simulated for the sizes 0.18 mm, 0.22 mm, and 0.33 mm, respectively, for pressure differentials ranging between 0.05 MPa to 22 MPa. Higher pressure differentials are used for the coarser particle sizes, which exhibit better plugging efficiency. Least-square error-based linear relationships were fitted for all the three particle sizes to obtain permeability values of 7.2E-13 m², 4.7E-13 m², and 7.6E-14 m², for 0.18 mm, 0.22 mm, and 0.33 mm particle sizes, respectively. It is evident from these simulations that coarser particles perform better at mouth-plugging.

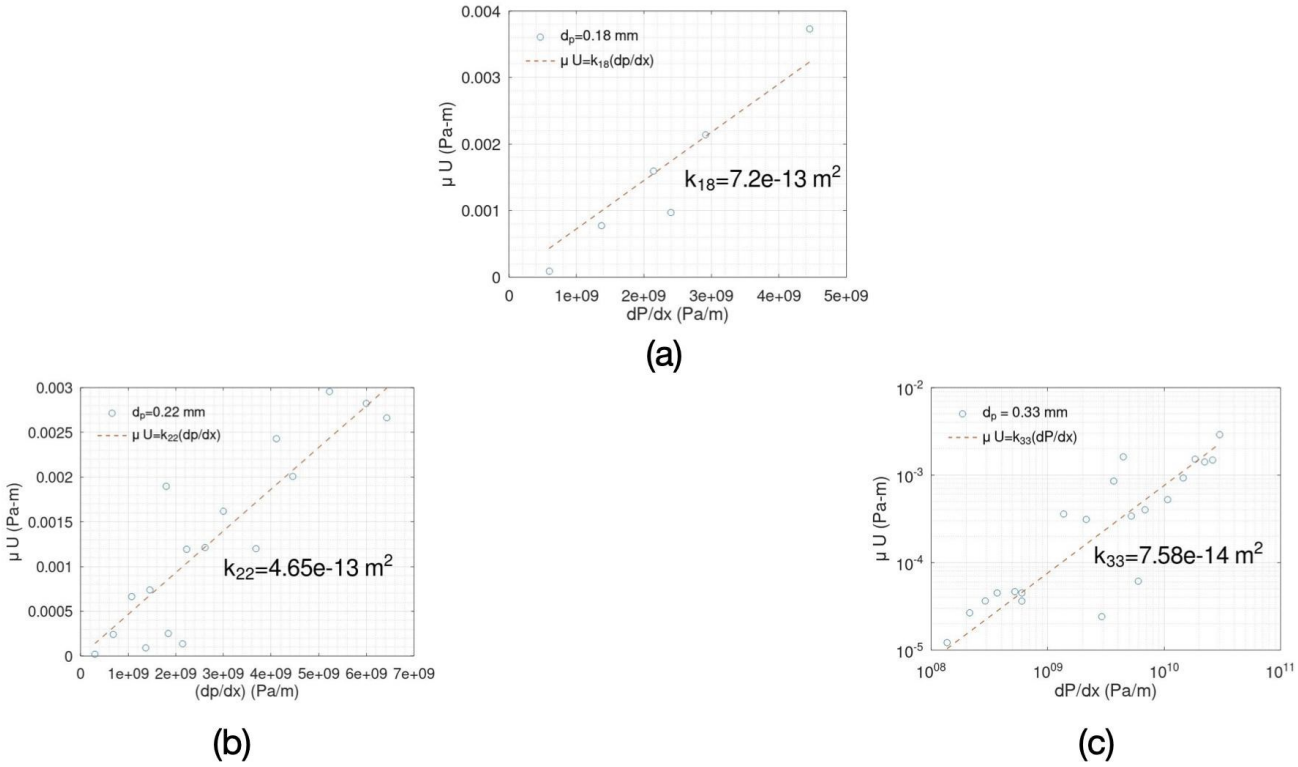

Figure 6: Linear fitting to derive effective time-averaged permeability values for cases with size (a) 0.18 mm, (b) 0.22 mm, and (c) 0.33 mm.

3. RESERVOIR-SCALE MODELING

3.1 NUMERICAL SIMULATOR

The numerical simulator used in this work was the TOUGH+ V1.5 (Moridis *et al*., 2014; Moridis & Freeman, 2014) core code with the RealGasBrine V1.0 option (T+RGB). A detailed description of the code and its capabilities can be found in manuals, available online (Moridis *et al*., 2014). For this study, we modify the T+RGB code to add a mud phase, adapting the code architecture used to represent dense brines. For density of the mud we implement the functions of Briscoe *et al*., (1994). For mud viscosity, we use relationships of Fisk *et al*., (1994). We adapt the results of the particle transport simulations by implementing a permeability reduction function that is applied to simulation elements subjected to infiltration by the drilling muds. The behavior of the mud is only treated in terms of the Darcy flow of the mud itself and the relevant fluid properties (density and viscosity of unadulterated mud), and the effect of the permeability reduction created by LCM in specific porous media (i.e. the fracture-dominated fluid-entry zones). Particle transport (i.e. filtering) is not considered in T+RGB, nor is shear-thinning behavior, and thus we simulate a worst-case scenario for leakage into the formation before permeability reductions are applied.

3.2 GEOLOGICAL AND COMPUTATIONAL MODELS

To create a generalized, schematic system to test permeability reductions, we use the Awibenkok Geothermal Field as well-characterized system (Hulen & Lutz, 1999; Hulen *et al*. 2000). The properties of the AWI 1-2 corehole are simplified to generate the geological model shown in Figure 4, where a 10 m fluid-entry (FE) zone is layered between low-permeability muds. Porosities of fluid-entry zones are averaged from associated datasets (Boitnott & Hulen, 2001) and permeabilities and other porous media properties are estimated as bulk properties of various layers. The physical properties used in the simulations are given in Table 1.

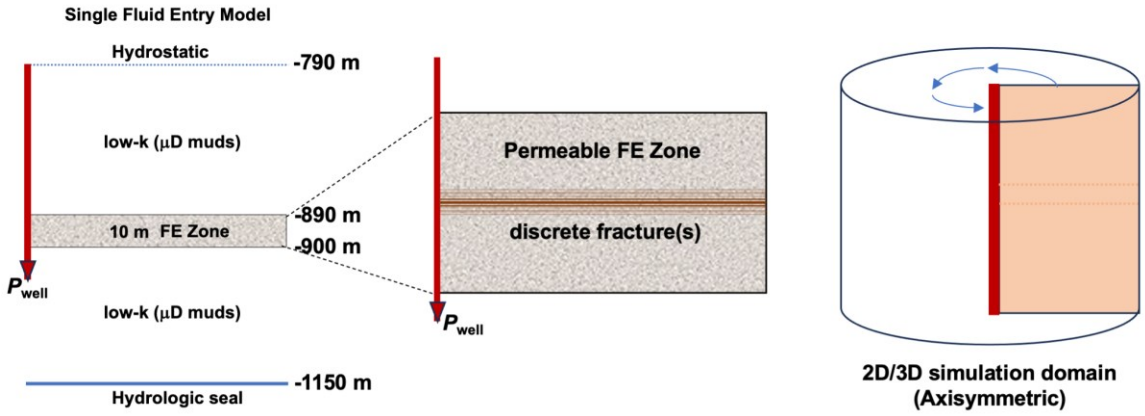

Figure 4: Geological model for the fluid-entry scenarios.

We consider two types of fluid-entry (FE) zone. 1) A homogeneous region of increased permeability within the layers of low-permeability mud/clay lahar layers ("single fluid entry" or SFE), which we define as a 10 m zone of increased permeability (due to fracturing within the layer,) similar to that found in the Awibenkok 1-2 well example. 2) A permeable FE zone with an additional discrete fractured layer, a 1 m zone with the 10 m FEZ populated with fractures of average aperture □ = 0.75 mm, corresponding to the fracture aperture used in Section 2. The effective permeability of these fractures is computed using the field-validated modified cubic-law formulation of Li *et al.* (2022) that accounts for "clustering" of multiple interconnected fractures.

For a vertical well and homogeneous properties within layers, we use an axisymmetric cylindrical mesh–a cylinder of radius 250 m. Discretization in r is logarithmic, with 100 elements from □r = 0.2 m (wellbore radius) to 10 m. A constant-P boundary condition is applied at r = 250 m. There are 64 layers in z, with vertical discretization □z = 1 m within the FE zone and an arithmetic progression of □z increasing above and below the FE zone to 26.4 m. A hydrological seal exists at the bottom of the system (z = -1150 m) and the top boundary (z = -790 m) is hydrostatic. The wellbore is modeled as a cylinder of radius 0.2 m. The overpressure of the circulating fluids is represented by a constant-P element at the bottom of the modeled wellbore set at a bottomhole pressure (BHP) of 9.96 MPa, a ~1.2 MPa overbalance. Simulations were run for up to 30 days with flow into the formation beginning at t = 0. We monitor total flow rate Q into adjacent formations through the wall of the wellbore, wellbore pressure P (adjacent to the FE zone), and the spatial evolution of the multiple fluid phases within the system.

Table 1: Computational Parameters

Lahar/mud k_r, k_z, □	10^{-18} m^2, 10^{-19} m^2, 0.12
Fluid-entry zone k_r, k_z, □	10^{-13} m^2, 10^{-14} m^2, 0.02
SFE+F fracture aperture □	0.75 mm
Initial pressure @ z = -790 m, -890 m	7.96 MPa, 8.73 MPa (hydrostatic)
Wellbore/Mud P, T	9.96 MPa, 100°C
Formation brine X_S	1.3 wt%
Pore compressibility (FEZ, Lahar)	10^{-10}, 10^{-8}
Grain density	2600 kg/m^3
Rock specific heat	1000 J/kg K

3.3 RESULTS AND DISCUSSION

Evolution of the total flow rate out of the wellbore into adjacent layers/zones Q is shown in Figure 5(a), for the cases of 1) the single FE zone and 2) the FE zone with a discrete fracture. Without LCM present, flow into adjacent formations is controlled only by the viscosity of the mud and the permeability of the FEZ and bounding layers, resulting in a loss of 200-300 BBL/hr at t = 1 min, and 160-260 BBL/hr after 15 min. Use of the 0.33 mm LCM reduces these flows significantly, with the permeability reduction appearing after t = ~1 min, reducing the flow rates to 60-110 BBL/hr. Flow rates would continue to decline from t = 15 min to t = 1 d (if circulation is allowed to continue) to 20-30 BBL/hr or less, as the LCM are emplaced within the FEZ.

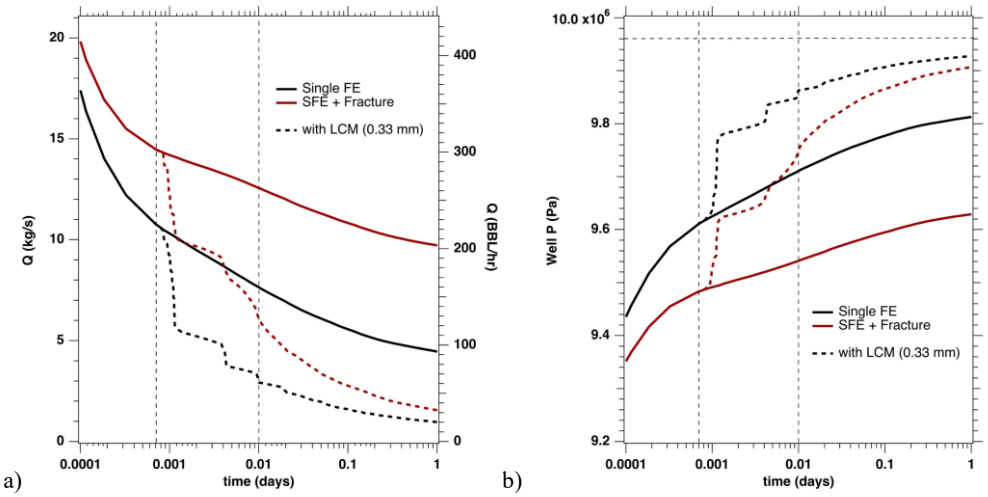

Figure 5: a) Total flow Q into the formation from the wellbore for 1) the SFE case, 2) the SFE + Fracture case, and 3) each with LCM present, and b) pressure in the wellbore for each case. Vertical dashed lines denote *t* = 60 s and *t* = 15 min on the log scale.

The permeability reduction results in a recovery of wellbore pressure after the initial pressure drop caused by rapid initial inflows into the FEZ, as seen in Figure 5(b). After an initial pressure drop of over 6 bar, wellbore pressure recovers to within ~1-2 bar of the original overpressure within 15 min, and could recover to within 0.3 to 0.5 bar after 1 day if circulation continued.

As calculated in Section 2, the size of the LCM grains can lead to order-of-magnitude changes in the final permeability of the porous medium due to the formation of stable bridges at the entrance of the fracture. Figure 6 compares (a) the flow rates Q and (b) wellbore pressure P for the three particle sizes vs. the SFE + Fracture scenario. The order-of-magnitude difference in permeability results in a range of Q from 58% of free-flow to 15%. This is most relevant to the recovery of pressure within the wellbore. In Figure 6(b), we see that P may recover to within 1-2 bar of initial overbalance pressure within t = 15 min for all LCM sizes, but only the largest particles (and their sustained permeability reduction) reduce this to 0.3 - 0.5 bar within 1 day. The smaller LCM may provide similar pressure recovery in the short term (15 min), but less effective pressure maintenance at longer times, due to the reduced permeability reduction and an effective permeability 10X greater, due to the fracture-bridging behavior described in Section 2.

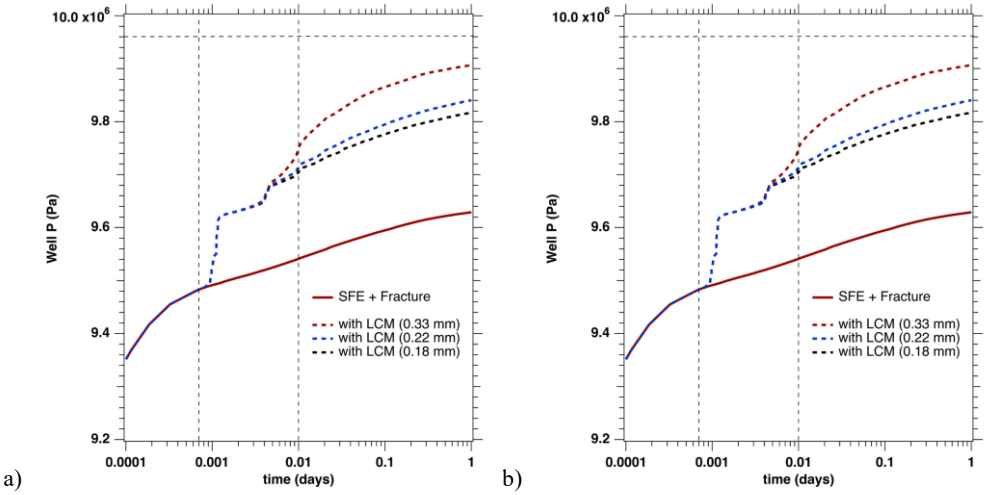

Figure 6: a) Total flow Q into the formation from the wellbore for the SFE + Fracture case, 1) without LCM and 2) with the three LCM choices, and b) pressure in the wellbore for each case. Vertical dashed lines denote *t* = 60 s and *t* = 15 min on the log scale.

4. CONCLUSIONS

Our grain-scale simulations of pressure-driven LCM flow near the entry of a fracture show unstable mouth-plugging behavior. The mechanism of mouth-plugging is via formation of and breakage of bridges periodically at the fracture opening. The cumulative fluid leakage through the fracture opening is characterized by a sequence of bridge formation and breakage events. For holding pressures ranging from 0.05 MPa to 22 MPa our 2D simulations result in single fracture permeability values of 7.2E-13 m^2, 4.7E-13 m^2, and 7.6E-14 m^2, for particle sizes of 0.18 mm, 0.22 mm, and 0.33 mm, respectively. The use of effective particulate LCMs can allow reduction of flows into formations adjacent to the well on timescales of minutes to hours. These reductions of fluid flow allow recovery of wellbore

pressure (and thus circulation) to permit continued drilling operations. Selection of the appropriate LCM, in this case by choosing a particle size that maximizes permeability reduction, is key to both the rapidity and magnitude of the recovery process.

ACKNOWLEDGEMENTS

This work was supported by the U.S. Department of Energy, Office of Energy Efficiency and Renewable Energy (EERE), Geothermal Technologies Office (GTO), under Award Number DE-AC02-05CH11231 with LBNL.

REFERENCES

Abrams, A. 1977 Mud design to minimize rock impairment due to particle invasion. Journal of Petroleum Technology 29 (05), 586–592.

Alsaba, Mortadha, Al Dushaishi, Mohammed F, Nygaard, Runar, Nes, Olav-Magnar & Saasen, Arild 2017 Updated criterion to select particle size distribution of lost circulation materials for an effective fracture sealing. Journal of Petroleum Science and Engineering 149, 641–648.

Andrade, José E., Lim, Keng-Wit, Avila, Carlos F. & Vlahinić, Ivan 2012 Granular element method for computational particle mechanics. Computer Methods in Applied Mechanics and Engineering 241-244, 262–274.

Bhuvankar, Pramod, Cihan, Abdullah & Birkholzer, Jens 2022 Pore-scale cfd simulations of clay mobilization in natural porous media due to fresh water injection Chemical Engineering Science 247, 117046.

Bhuvankar, Pramod, Cihan, Abdullah & Birkholzer, Jen T. 2023 Pore-scale analysis LCM Transport Modeling of the permeability damage and recovery during cyclic freshwater and brine injection in porous media containing non-swelling clays. Energies 16 (22).

Boitnott, GN & Hulen, JB 2001 Petrographic controls on electrical properties of core samples from the Awibengkok Geothermal Field, Indonesia. TRANSACTIONS-GEOTHERMAL RESOURCES COUNCIL pp. 391–394.

Briscoe, BJ, Luckham, PF & Ren, SR 1994 The properties of drilling muds at high pressures and high temperatures. Philosophical Transactions of the Royal Society of London. Series A: Physical and Engineering Sciences 348 (1687), 179–207.

Feng, Yongcun & Gray, K.E. 2017a Review of fundamental studies on lost circulation and wellbore strengthening. Journal of Petroleum Science and Engineering 152, 511–522.

Feng, Yongcun & Gray, K. E. 2017b Modeling lost circulation through drilling- induced fractures. SPE Journal 23 (01), 205–223.

Fisk, JV & Jamison, DE 1989 Physical properties of drilling fluids at high temperatures and pressures. SPE Drilling Engineering 4 (04), 341–346.

Hulen, JB & Lutz, SJ 1999 Alteration mineralogy and zoning in corehole AWI 1-2, Awibengkok geothermal system, West Java, Indonesia. TRANSACTIONS-GEOTHERMAL RESOURCES COUNCIL pp. 19–24.

Hulen, JB, Stimac, JA & Sugiaman, Fransiskus 2000 The AWI 1-2 core research program:part ii, stratigraphy, volcanic facies, and hydrothermal alteration. In Proceedings of the World Geothermal Congress, pp. 1271–1276.

Jeennakorn, Montri, Nygaard, Runar, Nes, Olav-Magnar & Saasen, Arild 2017 Testing conditions make a difference when testing lcm. Journal of Natural Gas Science and Engineering 46, 375–386.

Kang, Yili, Ma, Chenglin, Xu, Chengyuan, You, Lijun & You, Zhenjiang 2023 Prediction of drilling fluid lost-circulation zone based on deep learning. Energy 276, 127495.

Kibikas, William, Nakagawa, Seiji, Ingraham, Mathew, Bauer, Stephen, Chang, Chun, Dobson, Patrick, Kneafsey, Timothy & Samuel, Abraham 2024 Evaluation of lost circulation material sealing for geothermal drilling. Energies 17 (11).

Lashkari, Reza, Tabatabaei-Nezhad, Seyyed Alireza & Husein, Maen M. 2023 Evaluation of shape memory polyurethane as a drilling fluid lost circulation and fracture plugging material. Geoenergy Science and Engineering 222, 211445.

Lee, Lu & Dahi Taleghani, Arash 2020 Simulating fracture sealing by granular lcm particles in geothermal drilling. Energies 13 (18).

Lee, Lu & Dahi Taleghani, Arash 2022 Assessment of lost circulation material particle size distribution on fracture sealing: A numerical study. SPE Drilling & Completion, 191–205, arXiv: https://onepetro.org/DC/article-pdf/37/03/191/2995302/spe-209201-pa.pdf.

Lee, Lukas Jyuhn-Hsiarn & Taleghani, Arash Dahi 2021 Impact of particle size distribution on fracture sealing capability; a simulation for better geothermal drilling.

Li, Z., Sherman, Christopher S, Reagan, Matthew T, Moridis, George J & Morris, Joseph P 2022 Effects of heterogeneous fracture aperture on multiphase production from shale reservoirs. Transport in Porous Media 144 (3), 797–823.

Lin, Chong, Taleghani, Arash Dahi, Kang, Yili & Xu, Chengyuan 2022 A coupled cfd-dem simulation of fracture sealing: Effect of lost circulation material, drilling fluid and fracture conditions. Fuel 322, 124212.

Lin, Chong, Xu, Qi-Cong, Han, Lie-Xiang, Li, Gao, He, Hai, Zhou, Hong-Ling & She, Ji-Ping 2024 Fracture sealing performance of granular lost circulation materials at elevated temperature: A theoretical and coupled cfd-dem simulation study. Petroleum Science 21 (1), 567–581.

Loeppke, Gelan E., Glowka, David A. & Wright, Elton K. 1990 Design and evaluation of lost-circulation materials for severe environments. Journal of Petroleum Technology 42 (03), 328–337, arXiv: https://onepetro.org/JPT/article-pdf/42/03/328/2221519/spe-18022-pa.pdf.

Moridis, G 2014 User's manual of the TOUGH+ Core Code v1. 5: A general-purpose simulator of non-isothermal flow and transport through porous and fractured media. https://tough.lbl.gov/

Moridis, GJ & Freeman, CM 2014 User's manual for the RealGasBrine v1. 0 option of TOUGH+ v1. 5: A code for the simulation of system behavior in gas-bearing geologic media. https://tough.lbl.gov/

Nazemi, Rasoul, Moghadasi, Jamshid & Ashoori, Siavash 2024 Design and experimental study on rheological behavior and sealing performance of shear sensitive fluids to control lost circulation during drilling. Geoenergy Science and Engineering 237, 212830.

Nosewicz, S., Rojek, J., Chmielewski, M., Pietrzak, K. & Lumelskyj, D. 2017 Application of the hertz formulation in the discrete element model of pressure-assisted sintering. Granular Matter 19 (16).

Razavi, Omid, Karimi Vajargah, Ali, van Oort, Eric, Aldin, Munir & Govindarajan, Sudarshan 2016 Optimum particle size distribution design for lost circulation control and wellbore strengthening. Journal of Natural Gas Science and Engineering 35, 836–850.

SUN, Jinsheng, BAI, Yingrui, CHENG, Rongchao, LYU, Kaihe, LIU, Fan, FENG, Jie, LEI, Shaofei, ZHANG, Jie & HAO, Huijun 2021 Research progress and prospect of plugging technologies for fractured formation with severe lost circulation. Petroleum Exploration and Development 48 (3), 732–743.

Vickers, Stephen, Cowie, Martin, Jones, Tom & Twynam, Allan J 2006 A new methodology that surpasses current bridging theories to efficiently seal a varied pore throat distribution as found in natural reservoir formations. Wiertnictwo, Nafta, Gaz 23 (1), 501–515